Rapid Communications

Driven thermal waves and determination of the thermal conductivity in a magnetized plasma

S. Karbashewski,[1] R. D. Sydora,[1] B. Van Compernolle,[2] and M. J. Poulos[2]
[1]*Department of Physics, University of Alberta, Edmonton, Alberta, Canada T6G 2E1*
[2]*Department of Physics and Astronomy, University of California, Los Angeles, California 90095, USA*

(Received 26 July 2018; published 12 November 2018; corrected 10 January 2019)

Results are presented from a basic heat transport experiment using a magnetized electron temperature filament that behaves as a thermal resonator. A small, crystal cathode injects low-energy electrons along the magnetic field into the afterglow of a large preexisting plasma forming a hot electron filament embedded in a colder plasma. A series of low amplitude, sinusoidal perturbations are added to the cathode discharge bias that create an oscillating heat source capable of driving thermal waves. Langmuir probe measurements demonstrate driven thermal oscillations and allow for the determination of the amplitude and parallel phase velocity of the thermal waves over a range of driver frequencies. The results conclusively show the presence of a thermal resonance and are used to verify the parallel thermal wave dispersion relation based on classical transport theory. A nonlinear transport code is used to verify the analysis procedure. This technique provides an alternative measure of the density normalized thermal conductivity, independent of the electron temperature.

DOI: 10.1103/PhysRevE.98.051202

There exists an unconventional class of waves known as thermal diffusion waves, or simply thermal waves, that are produced using sinusoidally, time-varying heat sources [1]. First observed by Ångström in 1862 [2], thermal waves remained largely unstudied for nearly a century due in part to their heavy spatial attenuation and limited technology. The first-order time derivative in the heat equation instead of the familiar second-order time derivative in the traditional wave equation gives thermal waves unique properties, such as infinite propagation speed and an accumulation-depletion law instead of a reflection-refraction law at boundaries [3]. However, following the approach of other authors [4], this Rapid Communication uses familiar wave terminology to describe equivalent thermal wave phenomena. Since the arrival of the laser a variety of techniques for observing thermal waves in condensed and gaseous matter have been developed, with an emphasis on diagnostic applications [3]. These recent advancements resulted in the construction of thermal wave resonator cavities (TWRCs) [4] capable of sustaining quasistanding thermal waves. Driven thermal resonators in conjunction with frequency and cavity length scanning [5] have been used to measure the thermal properties of solids [6], liquids [7], and gases [8]. The success of TWRC diagnostic techniques with different forms of matter motivates the application of similar methods to magnetized plasmas, where electron heat transport processes are a central research topic and of particular importance to magnetic confinement fusion devices [9].

In strongly magnetized plasmas the thermal conductivity parallel to the magnetic field, $\kappa_\parallel$, is numerically quite large and orders of magnitude larger than the transverse conductivity, $\kappa_\perp$ [10]; thus, effective study of heat transport in these conditions requires a large system that is much longer along the magnetic axis than across. Over the past two decades a number of experiments [11–17] investigating electron heat transport in magnetized plasmas have been conducted by injecting an electron beam into a large, cold, magnetized plasma creating a long, narrow, hot-electron temperature filament aligned along the magnetic field. The most recent experiments [15] reported that the filament behaves as a TWRC in the parallel direction and exhibits spontaneous thermal fluctuations meeting the conditions for a quarter-wavelength resonance. The conclusion of Ref. [15] suggests the development of oscillatory electron beam sources for probing anomalous transport phenomena with thermal waves; the results presented herein represent the first steps toward such diagnostic tools.

Using a similar setup, this Rapid Communication reports on the stimulated excitation of thermal waves in the filament using sinusoidal perturbations to the electron beam heat source. We conclusively demonstrate that there is indeed a thermal resonance by sweeping the driver frequency and measuring the resulting amplitude of the temperature oscillations. Additionally, the ability to trigger the oscillations allows precise measurement of the thermal wave dispersion relation and provides evidence of stimulated thermal waves in a magnetized plasma. A by-product of the dispersion verification is the density normalized thermal conductivity, $\kappa_\parallel/n$, can be measured directly from the axial phase shift.

The complex wave number of a parallel propagating (with respect to the magnetic field) thermal wave at frequency ω in a uniform magnetized plasma is derived from the Fourier transform of the thermal diffusion equation coupled to an oscillatory source and takes the form [1]

$$k_\parallel = (1+i)\sqrt{\frac{3\omega n}{4\kappa_\parallel}}. \tag{1}$$

For classical thermal transport governed by Coulomb collisions the parallel conductivity of a magnetized plasma is

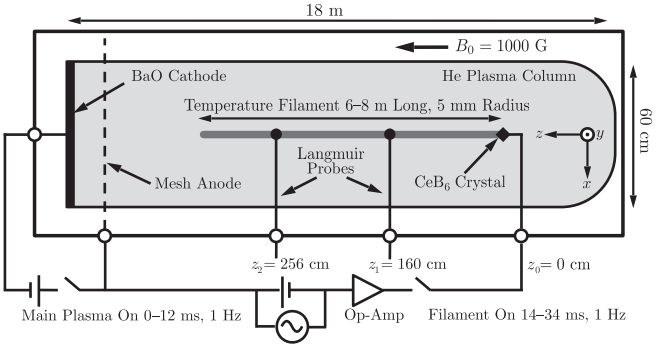

FIG. 1. Schematic (not to scale) of the experimental setup on the LAPD. In the afterglow phase of the main discharge the CeB_6 cathode injects an electron beam into the plasma, creating a temperature plume that is transported down the length of the device forming a narrow filament of elevated temperature. Langmuir probe measurements are made at axial positions $z_1 = 160$ cm and $z_2 = 256$ cm away from the filament heat source.

given by [10,18]

$$\kappa_\parallel = \frac{(3.16)nkT_e\tau_e}{m_e}, \tag{2}$$

where n is the plasma density (in cm^{-3}), k is Boltzmann's constant (in ergs/eV), T_e is the electron temperature (in eV), m_e is the electron mass (in g), the electron collision time (in s) is $\tau_e = (3.44\times10^5)T_e^{3/2}/(n\lambda)$, and λ is the Coulomb logarithm. Measurements of the parallel phase velocity of thermal fluctuations paired with independent measurements of the electron temperature and plasma density allow for confirmation of the real part of the dispersion relation in Eq. (1).

The experiments are performed in the Large Plasma Device (LAPD) operated by the Basic Plasma Science Facility (BaPSF) at the University of California, Los Angeles, which uses a magnetic field to confine a pulsed helium plasma to a cylindrical column that is 60 cm in diameter and 18 m in length along the magnetic axis [19]. The experimental setup is depicted in Fig. 1. The background magnetic field is fixed at $B_0 = 1$ kG for the results presented herein. The experiment lasts a total of 34 ms and has a high degree of reproducibility at a 1 Hz repetition rate. The main plasma column is generated using a hot barium oxide (BaO) cathode biased at ~ -70 V with respect to a mesh anode 50 cm away that injects electrons into the helium gas filling the chamber creating a plasma with $T_e \sim 6$ eV and $n_e \sim 1$–2×10^{12} cm^{-3}. The ion temperature is cooler having $T_i \lesssim 1$ eV. The main discharge lasts 12 ms at which point the bias is turned off and the plasma enters the afterglow phase where T_e rapidly decreases to ~0.25 eV; meanwhile, the density decays exponentially with a time constant on the order of tens of milliseconds.

A 3-mm-diameter crystal cathode of cerium hexaboride (CeB_6) is mounted on a probe shaft and inserted into the plasma a distance of 1500 cm from the BaO source; the crystal is continuously, ohmically heated with ~10 W of power. Starting 2 ms after the main discharge the crystal cathode is biased <20 V below the mesh anode for 20 ms, injecting thermionic electrons with energy below the ionization level

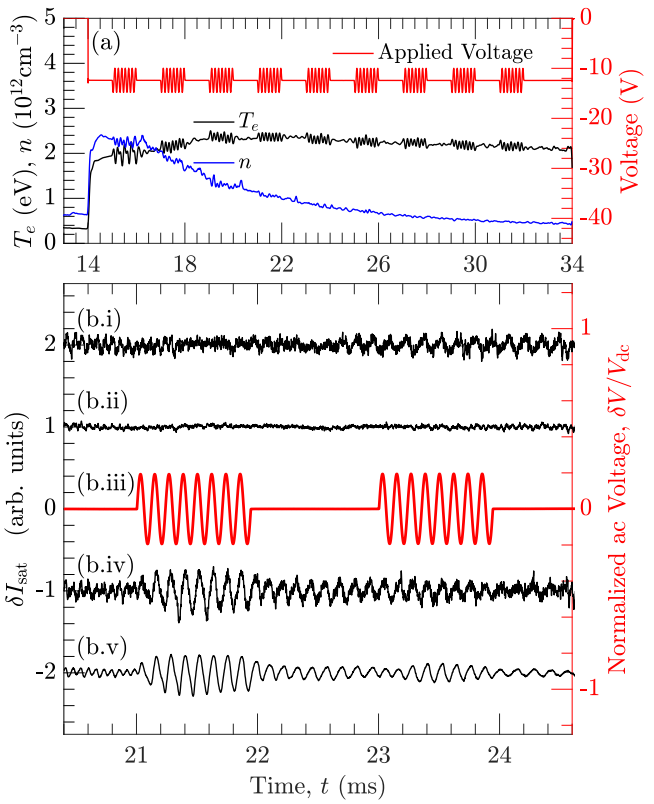

FIG. 2. (a) In black (middle) is the electron temperature, T_e, and in blue (bottom) the density, n, obtained from a Langmuir sweep for the applied voltage in red (top). (b) In black, δI_{sat} traces collected at z_2 depicting the spontaneous and stimulated thermal waves and in red the normalized applied voltage for ac shots. (i) Single dc shot, (ii) ten dc shots ensemble average, (iii) normalized applied voltage, (iv) single ac shot, and (v) 100 ac shots ensemble average.

of helium and a current <250 mA. The low-energy electron beam thermalizes in the region of plasma in front of the CeB_6 source creating a hot temperature plume <1 m in extent and a few millimeters in diameter [11]. Thermal transport rapidly conducts heat down the length of the device with minimal radial diffusion creating a region of elevated temperature 6–8 m in length with a symmetric, Gaussian-like transverse profile ~10 mm in diameter. The peak temperature near the heat source is 3–5 eV depending on the bias voltage and decreases continuously toward the end of the filament where the temperature equilibrates with the cold background plasma.

In the case of a dc bias applied to the CeB_6 cathode, the filament exhibits spontaneous thermal wave oscillations (~5–10 kHz) with a wavelength approximately equal to four times the filament length, as detailed in Ref. [15]. Using an operational amplifier, a modification is made to the filament biasing electronics to add a sinusoidal signal to the dc bias to create an oscillating heat source for driving thermal waves at arbitrary frequencies; this is shown in Fig. 1 by a simplified circuit schematic. The sinusoidal signal is added in the form of ten pulses ~1 ms long and spaced 1 ms apart; an example of this bias voltage is displayed in Fig. 2(a) with a 12.5 V dc offset, 2.5 V amplitude, and frequency of 7 kHz. Plasma shots with only a dc bias will be referred to as dc shots, and

those with sinusoidal pulse trains as ac shots. The ac shots are collected for a driver frequency range of $f_{ac} = 2$–50 kHz and an amplitude range of $\delta V/V_{dc} = 0.05$–0.40 where the long-time averaged temperature evolution is not perturbed. Thermal waves have large spatial attenuation; however, for typical filament parameters near the source, $T_e = 4$ eV, $n = 1\times10^{12}$ cm^{-3}, the wavelength of the thermal waves is ~10–50 m for the frequency range investigated and thus will not experience significant axial attenuation over the length of the filament. Given the length of the filament structure, all experimental measurements are made in a near-field regime for thermal waves.

Small, flat Langmuir probes are inserted into the plasma chamber at axial locations $z_1 = 160$ cm and $z_2 = 256$ cm measured from the position of the CeB_6 cathode. The probes are mounted on probe drives capable of <1 mm spatial control of the probe tips inside the containment vessel. Two types of measurement techniques are used with the Langmuir probes. The first measures the ion saturation current, which is proportional to the density and square root of the electron temperature, $I_{sat} \propto n\sqrt{T_e}$ [20,21]. The I_{sat} measurements are sampled at 12.5 MHz, providing sufficient temporal resolution of the thermal oscillations in the range of 2–50 kHz. Often the I_{sat} measurements are converted to δI_{sat} by removing frequency content below ~1 kHz. In addition to I_{sat} measurements, high temporal resolution I-V curves are reconstructed from many shots over a range of probe voltages in order to separate the plasma density and electron temperature; however, these reconstructed Langmuir sweeps are time-consuming and impractical for collecting data at many driver frequencies.

The probes at z_1 and z_2 make all measurements at the center of the filament in the x-y plane located at ($x = 0$ mm, $y = 0$ mm). Ten dc shots of I_{sat} are collected and for all the ac driver frequencies and amplitudes 100 shots of I_{sat} are collected. Additionally, for a 7 kHz ac trial reconstructed Langmuir sweeps were obtained and the result from z_2 is shown in Fig. 2(a). Highly coherent temperature oscillations are triggered with each applied pulse while the density, with the exception of the first applied pulse, shows no coherent driving. We note that both the temperature and density appear to have been perturbed by the first applied pulse and have significant nonlinear characteristics; it is not presently understood what causes this result but it does not persist beyond the first pulse. Thus, this demonstrates the oscillating power input is indeed driving thermal fluctuations and coherent I_{sat} fluctuations triggered by the ac signal can be interpreted as purely thermal beyond the first pulse.

The black traces in Fig. 2(b) show δI_{sat} collected in the center of the filament for $V_{dc} = 4$ V [Figs. 2(b.i) and 2(b.ii)] and for $\delta V/V_{dc} = 0.20$ at 8.5 kHz [Figs. 2(b.iv) and 2(b.v)]. Figure 2(b.i) is a single dc shot showing the spontaneous thermal oscillations going unstable at $t \sim 22.5$ ms, while Fig. 2(b.ii) shows the ten shot ensemble average. The dc ensemble average shows very little fluctuation as the random shot-to-shot phase of the spontaneous oscillations results in a nearly zero average. Figures 2(b.iv) and 2(b.v) show a single ac shot and the 100 ac shot ensemble average, respectively. In Fig. 2(b.iv) temperature oscillations are clearly excited by the ac signal. The ensemble average in Fig. 2(b.v) demonstrates that the thermal oscillations show high shot-to-shot coherence

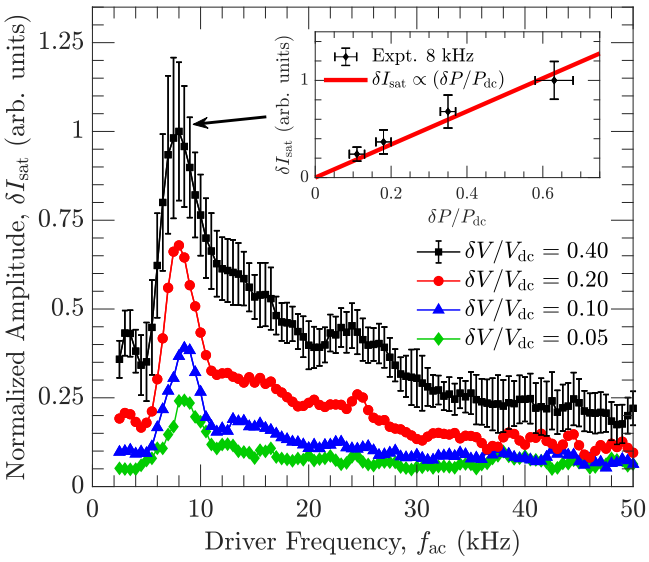

FIG. 3. Amplitude analysis of δI_{sat} at $z = z_2$ for different driver frequencies, f_{ac}, and amplitudes, $\delta V/V_{dc}$. The curves are all normalized to the maximum of $\delta V/V_{dc} = 0.40$ and the fractional error at $\delta V/V_{dc} = 0.40$ is similar for the other cases. Inset: the ~8 kHz amplitude resonance shows a linear scaling of δI_{sat} with respect to the amplitude of the oscillations in the driving power.

to the ac signal while other fluctuations are averaged out. The coherent oscillations between the applied pulses in Fig. 2(b.v) are due to the driver frequency matching the resonant frequency of the filament, detailed next, causing it to ring after the driver is removed.

Using the 100 ac shot ensemble averages the amplitude of the δI_{sat} fluctuations is measured for each driver frequency, f_{ac}; the result for the pulses from $t = 21$–22 ms is shown in Fig. 3 for different driver amplitudes. At 8 kHz there is a clear resonance in the amplitude of the thermal oscillations that closely matches the frequency of the spontaneous mode that develops in the dc shots, Fig. 2(b.i). Even at the lowest driver amplitude, $\delta V/V_{dc} = 0.05$, the resonance is distinct and demonstrates that even a small perturbation is capable of exciting the resonator. The quality factor of a resonator, Q, is defined as

$$Q = \frac{f_R}{\Delta f_R}, \quad \Delta f_R \equiv \text{FWHM}, \tag{3}$$

where f_R is the peak frequency of the resonance and Δf_R is the width of the resonance defined by the full width at half maximum (FWHM). For the resonance in Fig. 3 this corresponds to $Q \sim 2$, and is consistent with the low-quality factors associated with TWRCs in other forms of matter [4].

The inset of Fig. 3 shows the relationship at 8 kHz between δI_{sat} and the modulated input power to the heat source from the electron beam, $\delta P/P_{dc}$, which shows a linear dependence. This demonstrates that the amplitude of the resonant temperature oscillations scales linearly with the amplitude of the oscillating heat source, since to first order $\delta I_{sat} \propto \delta T_e$ when the oscillations are purely temperature, as established earlier. This $\delta T_e \propto \delta P$ relationship is consistent with the result of

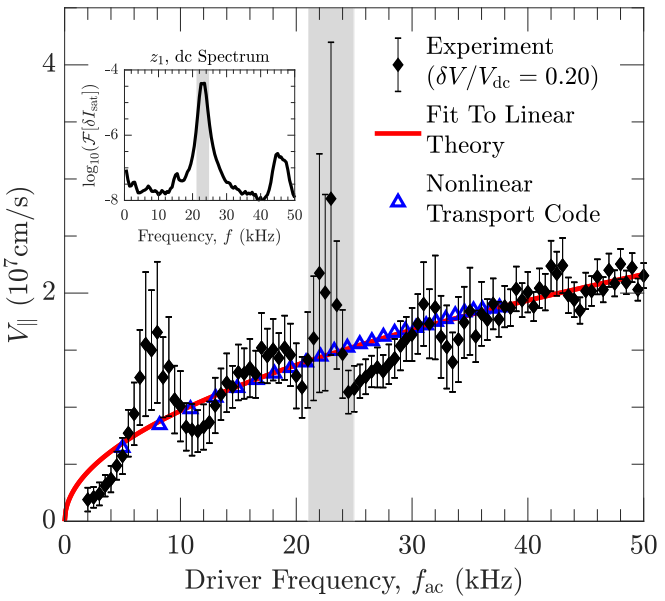

FIG. 4. The black diamonds are the experimentally measured phase velocity at different driver frequencies. A weighted least-square error fit of the data to Eq. (1) with $\kappa_\parallel/n$ as the fitting parameter is indicated by the red line. The result of a transport code used to model the linear analysis is denoted by hollow blue triangles. The inset figure is a spectral analysis of the signal at z_1 in the absence of driven oscillations.

a nonlinear transport code that models the experiment, described later.

Verification that the ac signal is driving thermal waves consistent with the dispersion relation in Eq. (1) is accomplished using the phase shift of the oscillations between z_1 and z_2. The axial phase shift of each pulse is calculated using the cross phase of the Fourier transform of the 100 ac shot ensemble averages collected at each location. The phase shift, distance $z_{12} = z_2 - z_1 = 96$ cm, and f_{ac} are used to compute the apparent phase velocity, $V_\parallel$ ($\equiv \omega/k_\parallel$), of the thermal waves. Figure 4 shows the result of this dispersion analysis as the relationship between $V_\parallel$ and f_{ac}. A weighted least-square error fit of the experimental data to Eq. (1) with $\kappa_\parallel/n$ as the fitting parameter, shown by the red curve, results in $\kappa_\parallel/n = (1.12 \pm 0.06)\times 10^9$ cm^2 s^{-1} and serves as an average along the path between z_1 and z_2. We compare this with a calculation using Eq. (2) and the average T_e and n from the Langmuir sweeps at z_1 and z_2 to arrive at $\kappa_\parallel/n = (1.6 \pm 0.5)\times 10^9$ cm^2 s^{-1}; these values are consistent when accounting for experimental uncertainty and confirm stimulated excitation of thermal waves. Lending strong support to this conclusion is the well-documented result that the axial transport in the filament follows classical transport theory [i.e., Eq. (2)] [11,13]. Additionally, this shows that $\kappa_\parallel/n$ can be measured accurately and independent of the electron temperature using this technique and suggests a future diagnostic application. During anomalous heat transport processes thermal wave diagnostics could be used when Eq. (2) is invalid.

There are two prominent features of the experimental data in Fig. 4, the first being the deviation at ~23 kHz and highlighted in gray. We note here that the error in the phase velocity comes from the standard deviation of the phase shifts calculated for individual shots at z_2 correlated with the average at z_1, and vice versa. The error in the data around ~23 kHz is much larger than elsewhere indicating low shot-to-shot consistency in the phase at those frequencies. The inset in Fig. 4 shows the Fourier transform of the dc shots at z_1 during the same time the ac pulses were applied; there is a distinct peak in the same region, also highlighted in gray, and a reduced amplitude harmonic. It has been previously reported that these are drift-Alfvén waves that develop due to the radial pressure gradient of the filament [14]. It is highly likely that the fundamental drift-Alfvén wave is impacting the ability to accurately measure the phase shift of the thermal waves in that frequency range.

The second deviation from the linear dispersion theory occurs in the region around ~7.5 kHz corresponding to the thermal resonance region discussed earlier; however, in the case presented in Fig. 4 the plasma parameters are marginally different than Fig. 3 and the thermal resonance peak occurs at ~5 kHz. The thermal wave dispersion theory assumes an infinite, uniform, thermally conducting medium away from the source and is incapable of describing a resonance. A finite model, as in other TWRCs, is required to include the proper boundary conditions with the ability to produce interference-equivalent phenomena in the thermal wave field [1,4,22]; in such models the phase and amplitude extrema do not always coincide, similar to our results. A more complete model to describe the phase and amplitude extrema not predicted by the simplest thermal wave field remains a work in progress.

The experiment uses a linear analysis to verify the dispersion; this method is supported by a nonlinear transport code used to model the experiment procedure. The transport code [23] evolves the nonlinear equations of continuity, momentum, and heat balance in cylindrical coordinates with assumed azimuthal symmetry. The nonlinear dependence of the thermal conductivities [10] is handled using an implicit split-tridiagonal scheme, detailed further in Ref. [23].

As previously mentioned, the electron beam heating is localized to a region immediately in front of the cathode. Numerically, the heating region is modeled as a spatially constant, ideal heat source with an adjustable input power. To obtain thermal waves in the code it is necessary to modulate the heat source with an ac signal in addition to a constant dc drive, which models the stimulated excitation in the experiment but contains no spontaneous excitation or resonance condition.

The validity of linear analysis for the experimental conditions considered can be verified with the transport code by repeating the calculation of the parallel phase velocity of thermal oscillations between two locations while varying the frequency. A measure of the expected nonlinear behavior can be deduced from the extent to which the code results match the predictions of the linear theory. The nonlinear transport code result in Fig. 4 clearly shows that the nonlinear dependence of the thermal conductivities plays a minor role for the conditions considered, providing further justification for the experimental procedure and analysis used in this study. We note that below 5 kHz the transport code does not accurately model sinusoidal thermal oscillations as seen in the experiment and the results there are omitted for this reason.

This Rapid Communication highlights new results on heat transport phenomena present in the magnetized electron temperature filament configuration that has previously been studied extensively [11–17]: First, the ability to stimulate excitation of parallel propagating thermal waves in a magnetized plasma using a modulated electron beam heat source has been clearly demonstrated. Second, using the thermal wave driver the spontaneous thermal mode observed previously [15] has been conclusively shown to correspond to a thermal resonance of the filament. Last, the dispersion relation verification provides a diagnostic technique for accurately measuring the density normalized parallel thermal conductivity, $\kappa_\parallel/n$, independent of the electron temperature.

We would like to thank Prof. George Morales for many helpful discussions and Trevor Karbashewski for his technical assistance in the design and construction of the circuit for modulating the electron beam. S.K. and R.D.S. acknowledge support from the Natural Sciences and Engineering Research Council of Canada (NSERC). The experiments were performed at the Basic Plasma Science Facility supported by DOE and NSF, with major facility instrumentation developed via an NSF Award No. AGS-9724366.

[1] A. Mandelis, in *Diffusion-Wave Fields: Mathematical Methods and Green Functions* (Springer, New York, 2001), Chap. 2, p. 2.
[2] A. J. Ångström, Ann. Phys. (NY) **190**, 513 (1862).
[3] A. Mandelis, Phys. Today **53**(8), 29 (2000).
[4] J. Shen and A. Mandelis, Rev. Sci. Instrum. **66**, 4999 (1995).
[5] J. Shen, A. Mandelis, and B. D. Aloysius, Int. J. Thermophys. **17**, 1241 (1996).
[6] D. Dadarlat, M. Streza, O. Onija, C. Prejmerean, L. Silaghi-Dumitrescu, N. Cobirzan, and K. Strzałkowski, J. Thermal Anal. Calorimetry **119**, 301 (2015).
[7] J. A. Balderas-López and A. Mandelis, Rev. Sci. Instrum. **72**, 2649 (2001).
[8] J. A. P. Lima, E. Marín, M. G. da Silva, M. S. Sthel, S. L. Cardoso, H. Vargas, and L. C. M. Miranda, Rev. Sci. Instrum. **72**, 1580 (2001).
[9] W. Horton, in *Turbulent Transport in Magnetized Plasmas* (World Scientific, Singapore, 2012), p. 338.
[10] S. I. Braginskii, in *Reviews of Plasma Physics*, edited by M. A. Leontovich (Consultants Bureau, New York, 1965), Vol. 1, p. 205.
[11] A. T. Burke, J. E. Maggs, and G. J. Morales, Phys. Rev. Lett. **81**, 3659 (1998).
[12] A. T. Burke, J. E. Maggs, and G. J. Morales, Phys. Plasmas **7**, 1397 (2000).
[13] A. T. Burke, J. E. Maggs, and G. J. Morales, Phys. Plasmas **7**, 544 (2000).
[14] A. T. Burke, J. E. Maggs, and G. J. Morales, Phys. Rev. Lett. **84**, 1451 (2000).
[15] D. C. Pace, M. Shi, J. E. Maggs, G. J. Morales, and T. A. Carter, Phys. Rev. Lett. **101**, 035003 (2008).
[16] D. C. Pace, M. Shi, J. E. Maggs, G. J. Morales, and T. A. Carter, Phys. Plasmas **15**, 122304 (2008).
[17] D. C. Pace, M. Shi, J. E. Maggs, G. J. Morales, and T. A. Carter, Phys. Rev. Lett. **101**, 085001 (2008).
[18] J. D. Huba, *NRL Plasma Formulary* (Naval Research Laboratory, Washington, DC, 2013), p. 37.
[19] W. Gekelman *et al.*, Rev. Sci. Instrum. **87**, 025105 (2016).
[20] F. F. Chen, Phys. Plasmas **8**, 3029 (2001).
[21] R. L. Merlino, Am. J. Phys. **75**, 1078 (2007).
[22] C. Wang, A. Mandelis, and Y. Liu, J. Appl. Phys. **96**, 3756 (2004).
[23] M. J. Poulos and G. J. Morales, Phys. Plasmas **23**, 092302 (2016).

Correction: The previously published Figure 4 contained inconsistent symbols and has been replaced.